# Low-momentum nucleon-nucleon interactions and shell-model calculations

L. Coraggio,[1] A. Covello,[1] A. Gargano,[1] N. Itaco,[1] D. R. Entem,[2] T. T. S. Kuo,[3] and R. Machleidt[4]
[1]*Dipartimento di Scienze Fisiche, Università di Napoli Federico II, and Istituto Nazionale di Fisica Nucleare, Complesso Universitario di Monte S. Angelo, Via Cintia-I-80126 Napoli, Italy*
[2]*Grupo de Física Nuclear, IUFFyM, Universidad de Salamanca, E-37008 Salamanca, Spain*
[3]*Department of Physics, SUNY, Stony Brook, New York 11794, USA*
[4]*Department of Physics, University of Idaho, Moscow, Idaho 83844, USA*
(Received 16 October 2006; published 27 February 2007)

In the last few years, the low-momentum nucleon-nucleon (*NN*) interaction $V_{\text{low-}k}$ derived from free-space *NN* potentials has been successfully used in shell-model calculations. $V_{\text{low-}k}$ is a smooth potential which preserves the deuteron binding energy as well as the half-on-shell $T$ matrix of the original *NN* potential up to a momentum cutoff $\Lambda$. In this paper, we test a new low-momentum *NN* potential derived from chiral perturbation theory at next-to-next-to-next-to-leading order with a sharp low-momentum cutoff at 2.1 fm$^{-1}$. Shell-model calculations for the oxygen isotopes using effective Hamiltonians derived from both types of low-momentum potential are performed. We find that the two potentials show the same perturbative behavior and yield very similar results.

DOI: 10.1103/PhysRevC.75.024311 PACS number(s): 21.30.Fe, 21.60.Cs, 27.20.+n, 27.30.+t

## I. INTRODUCTION

A challenging goal of nuclear structure theory is to perform shell-model calculations with single-particle (SP) energies and residual two-body interactions, both derived from a realistic nucleon-nucleon (*NN*) potential $V_{NN}$. To tackle this problem, a well-established framework is the time-dependent degenerate linked-diagram perturbation theory as formulated by Kuo, Lee, and Ratcliff [1,2], which enables the derivation of a shell-model effective Hamiltonian $H_{\text{eff}}$ starting from $V_{NN}$.

As is well known, a main feature of $V_{NN}$ is the presence of a built-in strong short-range repulsion dealing with high-momentum components of the potential. This hinders an order-by-order perturbative calculation of $H_{\text{eff}}$ in terms of $V_{NN}$, as the matrix elements of the latter are generally very large. However, in nuclear physics there is a natural separation of energy scales which can be used to formulate an advantageous theoretical approach for $V_{NN}$. As a matter of fact, the characteristic quantum chromodynamics (QCD) energy scale is $M_{\text{QCD}} \sim 1$ GeV, while for nuclear systems, we have $M_{\text{nuc}} \sim 100$ MeV [3].

This consideration was at the origin of the seminal work of Weinberg [4,5], who introduced into nuclear physics the method of effective field theory (EFT) to study the $S$ matrix for a process involving arbitrary numbers of low-momentum pions and nucleons. This approach is based on the known symmetries of QCD and parametrizes the unknown dynamical details introducing a number of constants to be determined.

Since then, much work has been carried out on this subject (see, for instance, Refs. [3,6–10]), leading to the construction of $V_{NN}$ based on chiral perturbation theory that are able to reproduce accurately the *NN* data [11,12]. However, these potentials also cannot be used in a perturbative nuclear structure calculation.

Inspired by EFT, a new approach based on the renormalization group (RG) has been recently introduced to derive a low-momentum *NN* interaction $V_{\text{low-}k}$ [13–15]. The starting point in the construction of $V_{\text{low-}k}$ is a realistic model for $V_{NN}$ such as the CD-Bonn [16], Nijmegen [17], Argonne $V18$ [18], or N$^3$LO [11] potentials. A cutoff momentum $\Lambda$ that separates fast and slow modes is then introduced, and from the original $V_{NN}$ an effective potential, satisfying a decoupling condition between the low- and high-momentum spaces, is derived by integrating out the high-momentum components. The main result is that $V_{\text{low-}k}$ is a smooth potential that preserves exactly the on-shell properties of the original $V_{NN}$ and is suitable to be used directly in nuclear structure calculations. In the past few years, $V_{\text{low-}k}$ has been fruitfully employed in microscopic calculations within different perturbative frameworks such as the realistic shell model [19–24], the Goldstone expansion for doubly closed-shell nuclei [25–27], and the Hartree-Fock theory for nuclear matter calculations [28–30].

The success of $V_{\text{low-}k}$ suggests that there may be a way to construct a low-momentum *NN* potential which is more deeply rooted in EFT and can be used in a perturbative approach. Namely, instead of taking the detour through a *NN* potential with high-momentum components, one may as well construct a low-momentum potential from scratch using chiral perturbation theory. We have constructed such a potential at next-to-next-to-next-to-leading order (N$^3$LO) using a sharp cutoff at 2.1 fm$^{-1}$. This potential reproduces the *NN* phase shifts up to 200 MeV laboratory energy and the deuteron binding energy. While $V_{\text{low-}k}$ allows only a numerical representation, the new low-momentum potential (dubbed N$^3$LOW) is given in analytic form. Moreover, the low-energy constants are explicitly known so that the chiral three-nucleon forces consistent with N$^3$LOW can be properly defined.

To investigate the perturbative properties of this new chiral low-momentum potential, we perform shell-model calculations for even oxygen isotopes. We employ two different effective Hamiltonians: one is based on the $V_{\text{low-}k}$ derived numerically from a "hard" N$^3$LO potential [11] and the other on N$^3$LOW.

 

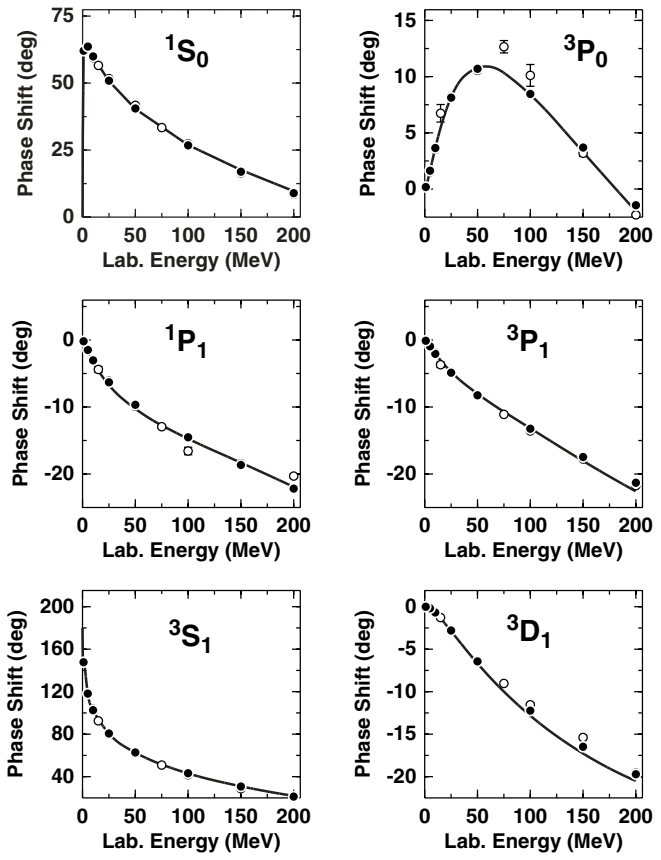


FIG. 1. Phase parameters of neutron-proton scattering up to 200 MeV laboratory energy for partial waves with total angular momentum $J \leqslant 2$. Predictions by the new low-momentum N$^3$LOW potential (solid lines). Data from the Nijmegen multienergy *np* phase shift analysis [35] (solid dots) and the GWU/VPI single-energy *np* analysis SM99 [36] (open circles).

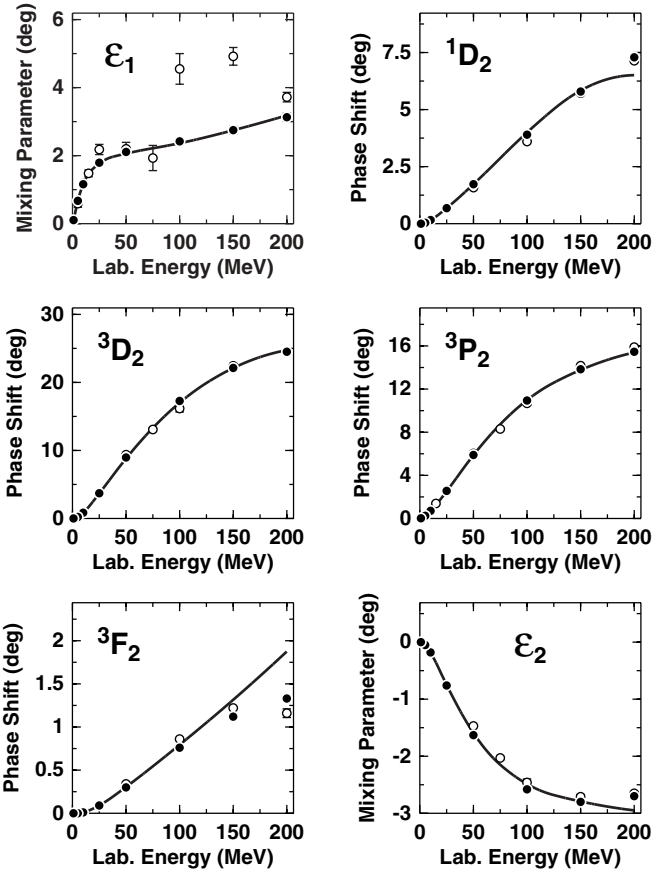


FIG. 2. Same as Fig. 1.

The paper is organized as follows. In Sec. II, we give a short description of how $V_{\text{low-}k}$ is derived as well as an outline of the construction of the N$^3$LOW potential. In Sec. III, a summary of the derivation of the shell-model $H_{\text{eff}}$ is presented with some details of our calculations. In Sec. IV, we present and discuss our results. Some concluding remarks are given in Sec. V.

## II. LOW-MOMENTUM NUCLEON-NUCLEON POTENTIALS

### A. Potential model $V_{\text{low-}k}$

First, we outline the derivation of $V_{\text{low-}k}$ [13–15]. As pointed out in the Introduction, the repulsive core contained in $V_{NN}$ is smoothed by integrating out the high-momentum modes of $V_{NN}$ down to a cutoff momentum $\Lambda$. This integration is carried out with the requirement that the deuteron binding energy and low-energy phase shifts of $V_{NN}$ are preserved by $V_{\text{low-}k}$. This is achieved by the following $T$-matrix equivalence approach. We start from the half-on-shell $T$ matrix for $V_{NN}$

$$T(k', k, k^2) = V_{NN}(k', k) + \mathcal{P}\int_0^\infty q^2 dq V_{NN}(k', q)\frac{1}{k^2 - q^2}T(q, k, k^2), \tag{1}$$

where $\mathcal{P}$ denotes the principal value and $k$, $k'$, and $q$ stand for the relative momenta. The effective low-momentum $T$ matrix

TABLE I. Ground-state energies (in MeV) of $^{18}$O relative to $^{16}$O calculated with $H_{\text{eff}}$ derived from the $V_{\text{low-}k}$ of the hard N$^3$LO potential as a function of the maximum number $N_{\max}$ of the HO quanta (see text for details). Results obtained at second and third order in perturbation theory are reported.

| $N_{\max}$ | 2 | 4 | 6 | 8 | 10 | 12 | 14 | 16 |
|---|---|---|---|---|---|---|---|---|
| 2nd | −5.572 | −8.191 | −10.615 | −12.748 | −14.318 | −15.037 | −15.142 | −15.168 |
| 3rd | −4.841 | −6.617 | −8.987 | −11.344 | −13.277 | −14.294 | −14.487 | −14.523 |

TABLE II. Same as Table I, but with $H_{\rm eff}$ derived from N$^3$LOW.

| $N_{\rm max}$ | 2 | 4 | 6 | 8 | 10 | 12 | 14 | 16 |
|---|---|---|---|---|---|---|---|---|
| 2nd | −2.568 | −4.806 | −6.789 | −9.085 | −11.759 | −13.671 | −14.108 | −14.162 |
| 3rd | −1.927 | −3.547 | −5.366 | −7.683 | −10.789 | −13.339 | −13.992 | −14.049 |

is then defined by

$$T_{\text{low-}k}(p', p, p^2) = V_{\text{low-}k}(p', p) + \mathcal{P}\int_0^\Lambda q^2 dq\, V_{\text{low-}k}(p', q) \times \frac{1}{p^2 - q^2} T_{\text{low-}k}(q, p, p^2), \quad (2)$$

where the intermediate state momentum $q$ is integrated from 0 to the momentum space cutoff $\Lambda$, and $(p', p) \leqslant \Lambda$. The above $T$ matrices are required to satisfy the condition

$$T(p', p, p^2) = T_{\text{low-}k}(p', p, p^2); \quad (p', p) \leqslant \Lambda. \quad (3)$$

The above equations define the effective low-momentum interaction $V_{\text{low-}k}$, and it has been shown [14] that they are satisfied by the solution

$$V_{\text{low-}k} = \hat{Q} - \hat{Q}'\int \hat{Q} + \hat{Q}'\int \hat{Q}\int \hat{Q} - \hat{Q}'\int \hat{Q}\int \hat{Q}\int \hat{Q} + \cdots, \quad (4)$$

which is the well known Kuo-Lee-Ratcliff (KLR) folded-diagram expansion [1,2], originally designed for constructing shell-model effective interactions. In Eq. (4), $\hat{Q}$ is an irreducible vertex function whose intermediate states are all beyond $\Lambda$, and $\hat{Q}'$ is obtained by removing from $\hat{Q}$ its terms that are first order in the interaction $V_{NN}$. In addition to the preservation of the half-on-shell $T$ matrix, which implies preservation of the phase shifts, this $V_{\text{low-}k}$ preserves the deuteron binding energy, since eigenvalues are preserved by the KLR effective interaction. For any value of $\Lambda$, the low-momentum potential of Eq. (4) can be calculated very accurately using iteration methods. Our calculation of $V_{\text{low-}k}$ is performed by employing the iteration method proposed in Ref. [31], which is based on the Lee-Suzuki similarity transformation [32].

The $V_{\text{low-}k}$ given by the $T$-matrix equivalence approach mentioned above is not Hermitian. Therefore, an additional transformation is needed to make it Hermitian. To this end, we resort to the Hermitization procedure suggested in Ref. [31], which makes use of the Cholesky decomposition of symmetric positive definite matrices.

### B. Potential model N$^3$LOW

The general and fundamental reason why the $V_{\text{low-}k}$ approach to nuclear structure physics works is that the dynamics ruling nuclear physics can be described in the framework of a low-energy EFT. This nuclear EFT is characterized by the symmetries of low-energy QCD, in particular, spontaneously broken chiral symmetry, and the degrees of freedom relevant for nuclear physics, nucleons and pions. The expansion based upon this EFT has become known as chiral perturbation theory ($\chi$PT), which is an expansion in terms of $(Q/M_{\rm QCD})^\nu$, where $Q$ denotes the magnitude of a nucleon three-momentum or a pion four-momentum, and $M_{\rm QCD}$ is the QCD energy scale [4,5]. For this expansion to converge at the proper rate, we have to have $Q \ll M_{\rm QCD}$. To enforce this, chiral $NN$ potentials are multiplied by a regulator function that suppresses the potential for nucleon momenta $Q > \Lambda$, with $\Lambda \ll M_{\rm QCD}$. Present chiral $NN$ potentials [11,12] typically apply values for $\Lambda$ around 2.5 fm$^{-1}$.

It is of course not accidental that the latter cutoff value is not too different from that typically used for $V_{\text{low-}k}$, namely, $\Lambda = 2.1$ fm$^{-1}$. This fact stimulates an obvious question: Is it possible to construct a chiral $NN$ potential with $\Lambda = 2.1$ fm$^{-1}$? Not surprisingly, the answer is in the affirmative.

Thus, we have constructed a $NN$ potential at N$^3$LO of chiral perturbation theory that carries a sharp momentum cutoff at 2.1 fm$^{-1}$. We have dubbed this potential N$^3$LOW.

One advantage of this potential is that it is given in analytic form. The analytic expressions are the same as for the "hard" N$^3$LO potential constructed by Entem and Machleidt in 2003 [11] and are given in Ref. [33]. Note that the procedure that needs to be followed to construct $V_{\text{low-}k}$ from a free $NN$ potential (cf. Sec. II A) can be carried out only numerically.

Another important issue are many-body forces. As demonstrated in Ref. [30], when applying a $V_{\text{low-}k}$ in certain nuclear many-body systems, the inclusion of a three-body force (3NF) may be crucial. For example, nuclear matter does not saturate without a 3NF when the two-nucleon force (2NF) is represented by a low-momentum potential. One great advantage of $\chi$PT is that it generates nuclear two- and many-body forces on an equal footing (for an overview of this aspect, see Ref. [34]). Most interaction vertices that appear in the 3NF and in the four-nucleon force (4NF) also occur in the 2NF. The parameters carried by these vertices are fixed in the

TABLE III. Same as Table I, but with experimental SP energies.

| $N_{\rm max}$ | 2 | 4 | 6 | 8 | 10 | 12 | 14 | 16 |
|---|---|---|---|---|---|---|---|---|
| 2nd | −12.269 | −12.201 | −12.000 | −11.847 | −11.771 | −11.750 | −11.748 | −11.749 |
| 3rd | −12.165 | −12.373 | −12.328 | −12.286 | −12.281 | −12.290 | −12.294 | −12.296 |

TABLE IV. Same as Table II, but with experimental SP energies.

| $N_{\max}$ | 2 | 4 | 6 | 8 | 10 | 12 | 14 | 16 |
|---|---|---|---|---|---|---|---|---|
| 2nd | −12.454 | −12.386 | −12.202 | −12.072 | −12.002 | −11.973 | −11.968 | −11.967 |
| 3rd | −12.440 | −12.663 | −12.637 | −12.612 | −12.656 | −12.722 | −12.737 | −12.739 |

construction of the chiral 2NF. Consistency requires that for the same vertices the same parameter values are used in the 2NF, 3NF, 4NF, etc. If the 2NF is analytic, these parameters are known, and there is no problem with their consistent proliferation to the many-body force terms. However, if a potential exists only in numeric form, then those parameters are not explicitly known, and the parameters to be used in the 3NF, 4NF, ... must be based upon educated guesses. The firm consistency between two- and many-body forces is lost. Moreover, if a potential is given only in numeric form, one does not know to what order of $\chi$PT it belongs. Thus, it is also not clear which orders of 3NF and 4NF to include to be consistent with the order of the 2NF.

Our newly constructed N$^3$LOW reproduces accurately the empirical deuteron binding energy, the experimental low-energy scattering parameters, and the empirical phase shifts of *NN* scattering up to at least 200 MeV laboratory energy, see Figs. 1 and 2. More details about this potential will be published elsewhere [37]. It is the main purpose of this paper to test if the perturbative properties of N$^3$LOW when applied in microscopic nuclear structure are as good as the ones of typical $V_{\text{low-}k}$ potentials.

## III. DERIVATION OF THE SHELL-MODEL EFFECTIVE HAMILTONIAN

In the framework of the shell model, an auxiliary one-body potential $U$ is introduced in order to break up the nuclear Hamiltonian into the sum of a one-body component $H_0$, which describes the independent motion of the nucleons, and a residual interaction $H_1$:

$$H = \sum_{i=1}^{A} \frac{p_i^2}{2m} + \sum_{i<j} V_{ij} = T + V$$
$$= (T + U) + (V - U) = H_0 + H_1. \qquad (5)$$

Once $H_0$ has been introduced, a reduced model space is defined in terms of a finite subset of $H_0$ eigenvectors. The diagonalization of the many-body Hamiltonian (5) in an infinite Hilbert space, which is obviously unfeasible, is then reduced to the solution of an eigenvalue problem for an effective Hamiltonian $H_{\text{eff}}$ in a finite space.

In this paper, we derive $H_{\text{eff}}$ by way of the time-dependent perturbation theory [1,2]. Namely, $H_{\text{eff}}$ is expressed through the KLR folded-diagram expansion in terms of the vertex function $\hat{Q}$ box, which is composed of irreducible valence-linked diagrams. We take the $\hat{Q}$ box to be composed of one- and two-body Goldstone diagrams through third order in $V$ [38]. Once the $\hat{Q}$ box has been calculated at this perturbative order, the series of the folded diagrams is summed up to all orders using the Lee-Suzuki iteration method [32].

The Hamiltonian $H_{\text{eff}}$ contains one-body contributions, which represent the effective SP energies. In realistic shell-model calculations, it is customary to use a subtraction procedure [39] so that only the two-body terms of $H_{\text{eff}}$ are retained – the effective interaction $V_{\text{eff}}$ – and the SP energies are taken from the experimental data.

In this work, we have followed a different approach by employing the theoretical SP energies obtained from the calculation of $H_{\text{eff}}$. This allows us to make a consistent study of the perturbative properties of the input potential $V$ ($V_{\text{low-}k}$ or N$^3$LOW) in the shell-model approach.

In this regard, it is worth pointing out that, owing to the presence of the $-U$ term in $H_1$, $U$-insertion diagrams arise in the $\hat{Q}$ box. In our calculation, we use as auxiliary potential the harmonic oscillator (HO), $U = \frac{1}{2}m\omega^2 r^2 + \Delta$, and take into account only the first-order $U$ insertion that appears in the collection of the one-body contributions, which is the dominant one [40].

## IV. RESULTS

We have performed shell-model calculations for even-mass oxygen isotopes beyond the doubly closed core $^{16}$O. Oxygen isotopes constitute a quite interesting nuclear chain, both theoretically and experimentally, and they have been considered a testing ground for realistic shell-model calculations since the pioneering work by Kuo and Brown [41]. Our calculations have been carried out by using the Oslo shell-model code [42].

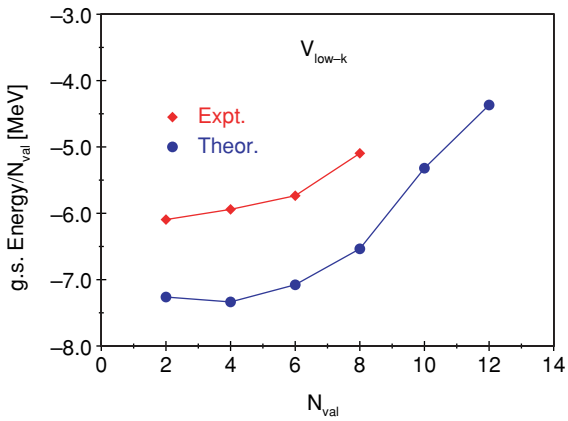


FIG. 3. (Color online) Experimental and calculated ground-state energy per valence neutron for even oxygen isotopes with $A$ from 18 to 28. $N_{\text{val}}$ is the number of valence neutrons. Calculated values are obtained with $H_{\text{eff}}$ derived from the $V_{\text{low-}k}$ of the hard N$^3$LO potential at third order in perturbation theory, with $N_{\max} = 16$.

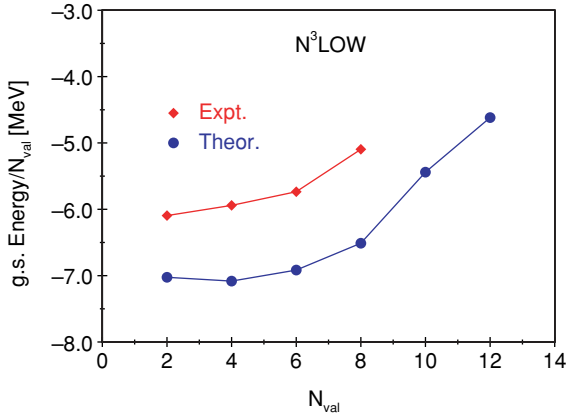


FIG. 4. (Color online) Same as Fig. 3, but with $H_{\text{eff}}$ derived from N$^3$LOW.

Two $H_{\text{eff}}$ have been obtained; for one of them, we used a $V_{\text{low-}k}$ with a cutoff momentum $\Lambda = 2.1$ fm$^{-1}$ derived numerically from the hard N$^3$LO chiral $NN$ potential [11], and for the other, the new N$^3$LOW potential described in Sec. II B. The Coulomb force between proton-proton intermediate states was explicitly taken into account. For the HO parameter $\hbar\omega$, we used the value of 14 MeV, as obtained from the expression $\hbar\omega = 45A^{-1/3} - 25A^{-2/3}$ [43] for $A = 16$. The value of $\Delta$ was chosen such that the self-energy and the $U$-insertion diagrams almost cancel each other [40]. The numerical value is $-54$ MeV, yielding an unperturbed energy of the $0s1d$ shell equal to $-5$ MeV, which is not far from the experimental value of the ground-state (g.s.) energy of $^{17}$O relative to $^{16}$O ($-4.144$ MeV [44]). However, it is worth noting that, when including only first-order $U$ insertions, our $H_{\text{eff}}$ matrix elements do not depend on the choice of $\Delta$.

The perturbative behavior of the input potential $V$ rules the convergence rate of the diagrammatic series for $H_{\text{eff}}$ which has to deal with the convergence of both the order-by-order perturbative expansion and the sum over the intermediate states in the Goldstone diagrams. In this context, we found it interesting to study and compare the convergence properties of $H_{\text{eff}}$ derived from both the $V_{\text{low-}k}$ and the N$^3$LOW potentials.

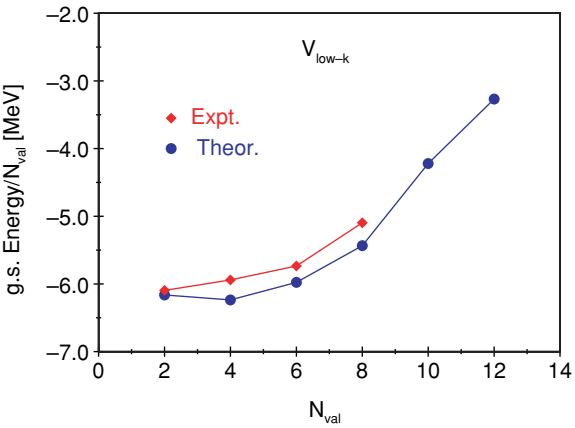


FIG. 5. (Color online) Same as Fig. 3, but with SP energies shifted upward by 1.1 MeV.

TABLE V. $J^\pi = 0^+$ TBME of $H_{\text{eff}}$ (in MeV) obtained from the $V_{\text{low-}k}$ of the hard N$^3$LO potential and N$^3$LOW at third order in perturbation theory with $N_{\max} = 16$. Compared with USDA TBME of Brown and Richter [45].

| Configuration | $V_{\text{low-}k}$ | N$^3$LOW | USDA |
|---|---|---|---|
| $(0d5/2)^2(0d5/2)^2$ | −2.435 | −2.689 | −2.480 |
| $(0d5/2)^2(0d3/2)^2$ | −3.464 | −3.741 | −3.569 |
| $(0d5/2)^2(1s1/2)^2$ | −1.269 | −1.337 | −1.157 |
| $(0d3/2)^2(0d3/2)^2$ | −0.845 | −1.147 | −1.505 |
| $(0d3/2)^2(1s1/2)^2$ | −0.862 | −0.967 | −0.983 |
| $(1s1/2)^2(1s1/2)^2$ | −2.385 | −2.563 | −1.846 |

In Table I, we present the $V_{\text{low-}k}$ g.s. energies of $^{18}$O relative to $^{16}$O obtained at second- and third-order perturbative expansion of $H_{\text{eff}}$. In both cases, the energies are reported as a function of the maximum allowed excitation energy of the intermediate states, expressed in terms of the oscillator quanta $N_{\max}$. It can be seen that the g.s. energy is practically convergent at $N_{\max} = 12$. As for the order-by-order convergence, it may be considered quite satisfactory, the difference between second- and third-order results being around 4% for $N_{\max} = 16$, which is the largest $N_{\max}$ we employed. Similar results are obtained using the N$^3$LOW potential, as shown in Table II. In this case, for $N_{\max} = 16$ the difference between second- and third-order results is less than 1%.

It is now worth commenting on the dimension of the intermediate state space. We have found that when increasing $N_{\max}$, the matrix elements of the two-body effective interaction $V_{\text{eff}}$ (TBME) are much more stable than the calculated SP energies. In this connection, the results obtained using experimental SP energies, shown in Tables III and IV, give evidence of the rapid convergence of the g.s. energy with $N_{\max}$. This supports the choice of moderately large intermediate state spaces in standard realistic shell-model calculations, where experimental SP energies are generally employed.

A comparison between the results obtained from the $V_{\text{low-}k}$ and the N$^3$LOW potentials (see Tables I and II, respectively) shows that at third order, with a sufficiently large number of intermediate states, the two interactions predict very close values for the relative binding energy of $^{18}$O. Note that the experimental value is $-12.187$ MeV [44]. From now on, we refer to calculations with $N_{\max} = 16$ and $\hat{Q}$-box diagrams up to third order in perturbation theory.

In Tables V and VI, we present the $J = 0^+$ TBME and the SP energies obtained from the $V_{\text{low-}k}$ and N$^3$LOW potentials.

TABLE VI. Calculated SP relative energies of $H_{\text{eff}}$ (in MeV) obtained from the $V_{\text{low-}k}$ of the hard N$^3$LO potential and N$^3$LOW at third order in perturbation theory with $N_{\max} = 16$. Compared with USDA SP energies of Brown and Richter [45] and experimental data. Values in parentheses are absolute SP energies.

| Orbital | $V_{\text{low-}k}$ | N$^3$LOW | USDA | Expt |
|---|---|---|---|---|
| $\nu 0d5/2$ | 0.0 (−5.425) | 0.0 (−4.909) | 0.0 (−3.944) | 0.0 (−4.144) |
| $\nu 0d3/2$ | 7.323 | 7.117 | 5.924 | 5.085 |
| $\nu 1s1/2$ | 1.257 | 0.818 | 0.883 | 0.871 |

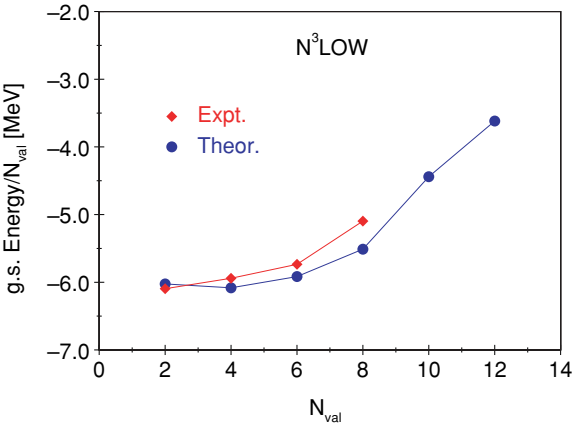


FIG. 6. (Color online) Same as Fig. 4, but with SP energies shifted upward by 1 MeV.

It turns out that the results from the two potentials are quite similar, the largest difference regarding the absolute energy of the $d_{5/2}$ SP level. In the last column of Tables V and VI, we also show the $J^\pi = 0^+$ TBME and SP energies obtained by Brown and Richter [45] from a least-squares fit of a large set of energy data for the *sd*-shell nuclei. The reported values refer to the USDA Hamiltonian, see Ref. [45] for details. It is interesting to note that the TBME of USDA are closer to ours than those of the original USD [46,47], which was based on a smaller set of data. Regarding the SP energies, we see that the USDA absolute energy of the $d_{5/2}$ state is in good agreement with the experimental g.s. state energy of $^{17}$O, while both our calculations give about 1 MeV more binding. On the other hand, our calculated and the USDA excitation energies of the $s_{1/2}$ state come close to each other and do not differ significantly from the experimental value. As for the relative energy of the $d_{3/2}$ state, the USDA value is larger than the experimental one, in line with our findings.

It is worth recalling that $H_{\rm eff}$, which was derived in the framework of the KLR approach, is defined for the two valence-nucleon problem. It is of interest, however, to test the theoretical SP energies, as given in Table VI, and the TBME in systems with many valence nucleons. To this end, we have calculated for even oxygen isotopes the g.s. energies relative to the $^{16}$O core up to $A = 28$, and the excitation energies

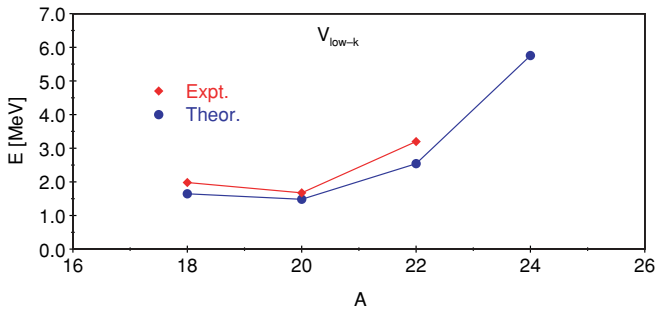


FIG. 7. (Color online) Experimental and calculated excitation energy of the first $2^+$ state for oxygen isotopes. Calculated values are obtained with $H_{\rm eff}$ derived from the $V_{\text{low-}k}$ of the hard N$^3$LO potential. Experimental data are from Ref. [53].

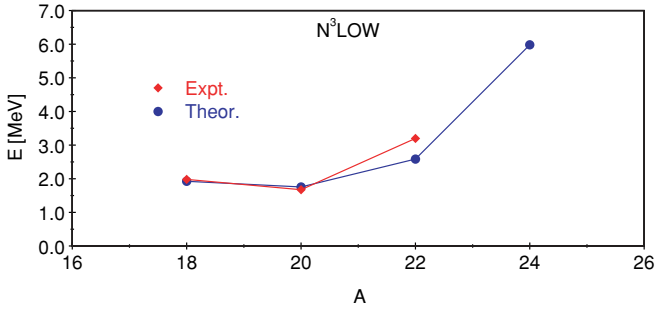


FIG. 8. (Color online) Same as in Fig. 7, but with $H_{\rm eff}$ derived from N$^3$LOW.

of the first $2^+$ state up to $A = 24$. In Figs. 3 and 4, the experimental g.s. energies per valence nucleon are compared with the calculated ones for the $V_{\text{low-}k}$ and the N$^3$LOW potential, respectively. The predictions from both potentials yield binding energies that are larger than the experimental ones, with the difference remaining almost constant when increasing the number of valence neutrons $N_{\rm val}$. In fact, if we shift the $V_{\text{low-}k}$ and N$^3$LOW SP spectra upward by 1.1 and 1 MeV, respectively, so as to reproduce the experimental $^{18}$O binding energy, then we obtain a very good agreement, as shown in Figs. 5 and 6.

This result is very interesting: our calculations fail to predict that $^{26}$O and $^{28}$O are unbound to two-neutron decay as indicated by experimental studies [48,49]. However, when the SP energies are shifted upward, then we obtain the correct binding properties, as seen from Figs. 5 and 6. Some recent papers [50,51] have argued that with a realistic shell-model interaction it is not possible to reproduce the correct behavior of the binding energy of oxygen isotopes. In Refs. [51,52], this has been ascribed to the lack of both genuine and effective three-body correlations. Our results suggest that a major factor is the lack of a real three-body force. In fact, as discussed above, we have obtained a good description of the binding energy of oxygen isotopes by modifying the SP spectrum so as to reproduce the g.s. energy of the two-valence nucleon $^{18}$O. The last quantity is obviously not affected by effective three-body correlations, but it is sensitive to genuine three-body forces.

In Figs. 7 and 8, we compare the experimental and calculated excitation energies of the first $2^+$ states for the $V_{\text{low-}k}$ and N$^3$LOW potential, respectively. In both cases, the experimental behavior as a function of $A$ is well reproduced.

## V. SUMMARY AND CONCLUSIONS

In this paper, we performed shell-model calculations employing an effective Hamiltonian obtained from a new low-momentum potential, dubbed N$^3$LOW, which is derived in the framework of chiral perturbation theory at next-to-next-to-next-to-leading order with a sharp cutoff at 2.1 fm$^{-1}$.

We studied the convergence properties of this potential by calculating the ground-state energy of $^{18}$O and compared the results with those obtained using the $V_{\text{low-}k}$ derived from the hard N$^3$LO potential of Entem and Machleidt [11]. It

turns out that the two low-momentum potentials show the same perturbative behavior. We also performed calculations for the heavier oxygen isotopes, obtaining binding energies that are very similar for the two potentials, but larger than the experimental ones. However, that by introducing an empirical shift of the SP spectrum the ground-state energies are well reproduced up to $^{24}$O, while $^{26}$O and $^{28}$O are unbound to two-neutron decay, in agreement with the experimental findings.

The main purpose of this work was to test the new chiral low-momentum *NN* potential N$^3$LOW. Unlike $V_{\text{low-}k}$, this potential has the desirable feature that it is given in analytic form. We have shown here that N$^3$LOW is suitable for perturbative applications in microscopic nuclear structure calculations and that it yields results which come quite close to those obtained from the $V_{\text{low-}k}$ derived from the hard N$^3$LO potential.

After this first successful application, there is now motivation to pursue further nuclear structure calculations with this new low-momentum potential.

## ACKNOWLEDGMENTS

This work was supported in part by the Italian Ministero dell'Istruzione, dell'Università e della Ricerca (MIUR), the U.S. DOE Grant No. DE-FG02-88ER40388, the U.S. NSF Grant No. PHY-0099444, the Ministerio de Ciencia y Tecnonología under Contract No. FPA2004-05616, and the Junta de Castilla y León under Contract No. SA-104/04.

[1] T. T. S. Kuo, S. Y. Lee, and K. F. Ratcliff, Nucl. Phys. **A176**, 65 (1971).
[2] T. T. S. Kuo and E. Osnes, *Lecture Notes in Physics* (Springer-Verlag, Berlin, 1990), Vol. 364.
[3] U. van Kolck, Prog. Part. Nucl. Phys. **43**, 337 (1999).
[4] S. Weinberg, Phys. Lett. **B251**, 288 (1990).
[5] S. Weinberg, Nucl. Phys. **B363**, 3 (1991).
[6] G. P. Lepage, in *Nuclear Physics: Proceedings of the VIII Jorge Andre' Swieca Summer School*, edited by C. A. Bertulani, M. E. Bracco, B. V. Carlson, and M. Nielsen (World Scientific, Singapore, 1997), p. 135.
[7] D. B. Kaplan, M. J. Savage, and M. B. Wise, Phys. Lett. **B424**, 390 (1998).
[8] E. Epelbaoum, W. Glöckle, and U.-G. Meissner, Nucl. Phys. **A637**, 107 (1998).
[9] *Nuclear Physics with Effective Field Theory II*, edited by P. F. Bedaque, M. J. Savage, R. Seki, and U. van Kolck (World Scientific, Singapore, 2000).
[10] W. C. Haxton and C. L. Song, Phys. Rev. Lett. **84**, 5484 (2000).
[11] D. R. Entem and R. Machleidt, Phys. Rev. C **68**, 041001(R) (2003).
[12] E. Epelbaum, W. Glöckle, and U.-G. Meissner, Nucl. Phys. **A747**, 362 (2005).
[13] S. Bogner, T. T. S. Kuo, and L. Coraggio, Nucl. Phys. **A684**, 432c (2001).
[14] S. Bogner, T. T. S. Kuo, L. Coraggio, A. Covello, and N. Itaco, Phys. Rev. C **65**, 051301(R) (2002).
[15] S. Bogner, T. T. S. Kuo, and A. Schwenk, Phys. Rep. **386**, 1 (2003).
[16] R. Machleidt, Phys. Rev. C **63**, 024001 (2001).
[17] V. G. J. Stoks, R. A. M. Klomp, C. P. F. Terheggen, and J. J. De Swart, Phys. Rev. C **49**, 2950 (1994).
[18] R. B. Wiringa, V. G. J. Stoks, and R. Schiavilla, Phys. Rev. C **51**, 38 (1995).
[19] L. Coraggio, A. Covello, A. Gargano, N. Itaco, and T. T. S. Kuo, Phys. Rev. C **66**, 064311 (2002).
[20] L. Coraggio, A. Covello, A. Gargano, N. Itaco, T. T. S. Kuo, D. R. Entem, and R. Machleidt, Phys. Rev. C **66**, 021303(R) (2002).
[21] L. Coraggio, A. Covello, A. Gargano, and N. Itaco, Phys. Rev. C **70**, 034310 (2004).
[22] L. Coraggio, A. Covello, A. Gargano, and N. Itaco, Phys. Rev. C **72**, 057302 (2005).
[23] L. Coraggio and N. Itaco, Phys. Lett. **B616**, 43 (2005).
[24] L. Coraggio, A. Covello, A. Gargano, and N. Itaco, Phys. Rev. C **73**, 031302(R) (2006).
[25] L. Coraggio, N. Itaco, A. Covello, A. Gargano, and T. T. S. Kuo, Phys. Rev. C **68**, 034320 (2003).
[26] L. Coraggio, A. Covello, A. Gargano, N. Itaco, T. T. S. Kuo, and R. Machleidt, Phys. Rev. C **71**, 014307 (2005).
[27] L. Coraggio, A. Covello, A. Gargano, N. Itaco, and T. T. S. Kuo, Phys. Rev. C **73**, 014304 (2006).
[28] J. Kuckei, F. Montani, H. Müther, and A. Sedrakian, Nucl. Phys. **A723**, 32 (2003).
[29] A. Sedrakian, T. T. S. Kuo, H. Müther, and P. Schuck, Phys. Lett. **B576**, 68 (2003).
[30] S. K. Bogner, A. Schwenk, R. J. Furnstahl, and A. Nogga, Nucl. Phys. **A763**, 59 (2005).
[31] F. Andreozzi, Phys. Rev. C **54**, 684 (1996).
[32] K. Suzuki and S. Y. Lee, Prog. Theor. Phys. **64**, 2091 (1980).
[33] D. R. Entem and R. Machleidt, Phys. Rev. C **66**, 014002 (2002).
[34] R. Machleidt and D. R. Entem, J. Phys. G **31**, S1235 (2005).
[35] V. G. J. Stoks, R. A. M. Klomp, M. C. M. Rentmeester, and J. J. de Swart, Phys. Rev. C **48**, 792 (1993).
[36] R. A. Arndt, I. I. Strakowsky, and R. L. Workman, George Washington University Data Analysis Center (formerly VPI SAID facility), solution of summer 1999 (SM99).
[37] D. R. Entem and R. Machleidt (to be published).
[38] T. T. S. Kuo, J. Shurpin, K. C. Tam, E. Osnes, and P. J. Ellis, Ann. Phys. (NY) **132**, 237 (1981).
[39] J. Shurpin, T. T. S. Kuo, and D. Strottman, Nucl. Phys. **A408**, 310 (1983).
[40] J. Shurpin, D. Strottman, T. T. S. Kuo, M. Conze, and P. Manakos, Phys. Lett. **B69**, 395 (1977).
[41] T. T. S. Kuo and G. E. Brown, Nucl. Phys. **85**, 40 (1966).
[42] T. Engeland, the Oslo shell-model code 1991–2006 (unpublished).
[43] J. Blomqvist and A. Molinari, Nucl. Phys. **A106**, 545 (1968).
[44] G. Audi, A. H. Wapstra, and C. Thibault, Nucl. Phys. **A729**, 337 (2003).
[45] B. A. Brown and W. A. Richter, Phys. Rev. C **74**, 034315 (2006).
[46] B. H. Wildenthal, Prog. Part. Nucl. Phys. **11**, 5 (1984).
[47] B. A. Brown and B. H. Wildenthal, Annu. Rev. Nucl. Part. Sci. **38**, 29 (1988).

[48] M. Fauerbach, D. J. Morrissey, W. Benenson, B. A. Brown, M. Hellström, J. H. Kelley, R. A. Kryger, R. Pfaff, C. F. Powell, and B. M. Sherrill, Phys. Rev. C **53**, 647 (1996).
[49] O. Tarasov, R. Allatt, J. C. Angélique, R. Anne, C. Borcea, Z. Dlouhy, C. Donzaud, S. Grévy, D. Guillemaud-Mueller, M. Lewitowicz *et al*., Phys. Lett. **B409**, 64 (1997).
[50] B. A. Brown, Prog. Part. Nucl. Phys. **47**, 517 (2001).
[51] P. J. Ellis, T. Engeland, M. Hjorth-Jensen, M. P. Kartamyshev, and E. Osnes, Phys. Rev. C **71**, 034301 (2005).
[52] A. P. Zuker, Phys. Rev. Lett. **90**, 042502 (2003).
[53] Data extracted using the NNDC On-line Data Service from the ENSDF database, file revised as of 30 May 2006.